Electrochimica Acta 533 (2025) 146468

Contents lists available at ScienceDirect

Electrochimica Acta

journal homepage: www.journals.elsevier.com/electrochimica-acta

Determination of battery separator permeability by scanning electrochemical microscopy

Simona De Zio [a,1], Giampaolo Lacarbonara [a,1], Wouter Badenhorst [b,1], Marco Malferrari [a], Rossella Petruzzelli [a], Lasse Murtomäki [b,*], Catia Arbizzani [a,*], Stefania Rapino [a,*]

[a] Department of Chemistry "Giacomo Ciamician", University of Bologna, via Piero Gobetti 85, 40129 Bologna, Italy
[b] Department of Chemistry and Materials Science, Aalto University, PO Box 16100, 00076, Aalto, Finland

ARTICLE INFO

Keywords:
Scanning electrochemical microscopy
Microelectrodes
Copper-based redox flow batteries
Separators

ABSTRACT

Separators are critical components in batteries. In closed systems, like lithium-ion batteries, they should ensure a good ion transport between the two electrodes. In open systems, such as flow batteries, separators should also avoid the crossover of the redox species in the flowing electrolytes. We focused our studies on separators for redox flow batteries (RFBs), which are widely applied as electrochemical energy storage systems, specifically in combination with renewable energy systems like photovoltaic or wind turbines. We pioneered the use of scanning electrochemical microscopy to characterize the efficiency of different commercial membranes, specifically for all-copper RFB, by evaluating the cupric ion permeation through these membranes. In fact, one drawback of this system is represented by the permeation of cupric ions in the negative half-cell that leads to the dissolution of the copper deposit and results in the battery's self-discharge. Several types of membranes have been tested as separators to limit this process. Finite elements simulations were also performed to quantitatively interpret the electrochemical measurements and to correlate separator permeabilities to membrane molecular characteristics such as hydrophobicity and ion exchange capability. Estimates of copper ion diffusion coefficients and permeabilities were provided for a subset of the separators investigated.

1. Introduction

1.1. Importance of membranes in redox flow batteries

The growing energy demand and the proliferation of renewable power sources have intensified the adoption of electrochemical energy storage systems. Among the various battery architectures, redox flow batteries (RFBs) are an ideal choice for large stationary applications [1]. In an RFB stack, constituted by several cells, the redox species are contained in the anolyte and catholyte, which are stored in two separate and external reservoirs. These solutions are pumped through the positive and negative compartments of the RFB cells, which are separated by a membrane [2]. The essential function of the membrane is to keep the redox couples contained in the anolyte and catholyte separated, allowing, at the same time, high-rate transport of the supporting electrolyte ions across the membrane. The membrane's selectivity is a key feature to limit the crossover of the redox species that could be involved in side-reactions and thus result in a low coulombic efficiency of the system, or in a decreased overall capacity of the RFB. RFB chemistry takes advantage of diverse redox couples and charge carriers, which also means that separators should have specific requirements in terms of ion transport properties [3–9]. Considering that most RFBs work in acidic media (e.g. HCl and H_2SO_4), an ideal membrane should offer enough chemical stability under acidic conditions, and electrochemical stability to oxidizing and reducing potentials. To prevent the crossover of the species, a membrane with low permeability of the active redox species is needed, which also blocks the preferential transfer of water. At the same time, the membrane should allow the transfer of the supporting electrolyte for maintaining electroneutrality and closing the circuit [10,11]. The most straightforward systems consist of porous membranes made of polymeric matrix of well-defined porosity, which have the advantage of being based on stable, low-cost polymers (e.g., polyethylene, polypropylene). Such membranes are only a physical barrier for the crossover of species, and the problem of ion selectivity is still unsolved.

* Corresponding authors.
E-mail addresses: lasse.murtomaki@aalto.fi (L. Murtomäki), catia.arbizzani@unibo.it (C. Arbizzani), stefania.rapino3@unibo.it (S. Rapino).
[1] These authors contributed equally to this work.

https://doi.org/10.1016/j.electacta.2025.146468
Received 23 January 2025; Received in revised form 12 May 2025; Accepted 13 May 2025
Available online 14 May 2025

The most used approach to increase the selectivity of the crossing species is the incorporation of charged functional groups in the polymeric chain. The resulting membranes are called Ion Exchange Membranes (IEM) [12]. Ion transport through IEMs is governed by the interaction between the membrane's fixed charged groups and mobile ions in solution. These membranes are composed of polymers functionalized with ionic groups, which act as exchange sites. When hydrated, the membrane forms microscopic channels filled with water, allowing ions to move through. The transport mechanism primarily involves ionic conduction eased by electrostatic interactions: oppositely, charged ions are attracted to the fixed groups, replacing mobile counter-ions. For cation-exchange membranes (CEMs), negative functional groups (as $–SO_3^-$, $–COO^-$, $–PO_3^{2-}$, $–PO_3H^-$, $–C_6H_4O^-$) selectively bind cations, enabling their transport while repelling anions. Conversely, anion-exchange membranes (AEMs) have positive functional groups (such as $–NH_3^+$, $–NRH_2^+$, $–NR_2H^+$, $–NR_3^+$, $–PR_3^+$, $–SR_2^+$) that selectively transfer cations [13–15].

Ion mobility within the membrane depends on several factors, including hydration level, pore size, and the strength of electrostatic interactions. Higher water uptake increases pore size and ion mobility but can also reduce selectivity by allowing co-ions or neutral molecules to pass through. Ion transport mechanisms include hopping processes, where ions move between adjacent sites by breaking and reforming hydration shells. As an example, for protons, the Grotthuss mechanism plays a significant role, involving rapid proton hopping along hydrogen bonds in the membrane's hydrated network [16].

1.2. Membrane test procedures

There are several key-indicators for assessing membrane performance [11,17–22]. Aside from chemical, thermal, mechanical and electrochemical stability, a good ionic transport through the membrane, i.e. high ionic conductivity, reduces ohmic polarization, with the resulting enhancement of cell (and battery) energy. In addition, low resistance allows the use of high currents, improving battery power. The ionic conductivity is related to the areal resistance of the membrane that can be measured by electrochemical impedance spectroscopy over a wide frequency range. The membrane permeability is usually evaluated by measuring the static diffusion of ions across the membrane that separates the two compartments of an H-cell with solution at different concentrations. In vanadium RFBs, UV–visible absorbance spectra of electrolyte samples at various times, allow the calculation of the concentration values by using Fick's and Lambert-Beer's laws. It must be considered that this approach is not suitable for highly concentrated solutions because the relationship between absorbance and concentration is no longer linear. Furthermore, the ion diffusion could be influenced by picking up electrolyte sample aliquots for the analysis due to generated convective motions in the cell.

Also swelling and electrolyte uptake, which are intrinsic properties of the polymer membrane in presence of a certain electrolyte solution, affect the ion transport through the membrane and can increase the unwanted permeability (crossover) of the redox species. Membranes with a higher selectivity, such as ion exchange membranes, may decrease crossover although sometimes at the expense of ion conductivity. Ion exchange capacity is an important parameter describing the ionic transport properties of an IEM, which is defined as the milliequivalent ion-exchange groups in a gram of dry membrane, and is usually evaluated in a static cell, just like ion permeability. These measurements characterize the performance of separators in the presence of a specific electrolyte system. Thus, they do not give any information about the selectivity of single redox species [23,24]. It is also possible to evaluate membrane overall performance in a redox flow cell by galvanostatic charge and discharge cycles. Even if these tests are mandatory when evaluating membranes, galvanostatic charge and discharge cycles are influenced by many other parameters (e.g., charge transfer resistances, adhesion problems at the current collectors, chemical stability of the cell components, parasitic reactions at the electrodes). In addition, membrane behavior inside RFB depends on operation parameters like temperature and electrolyte flow and composition. For this reason, electrochemical cell tests give only a comparative and indirect evaluation of membrane performance [22,25].

1.3. Scanning electrochemical microscopy for permeation studies

Scanning electrochemical microscopy (SECM) can be a powerful technique to investigate the permeability of the membranes. SECM employs microelectrodes as probes to get electrochemical information while approaching or scanning the surface of the substrate of interest [26]. The use of microelectrodes offers several advantages for electrochemical measurements (e.g. the possibility to characterize micro-domains, fast steady-state achievement of the signal and diminished ohmic potential drop). The precise positioning of the probe, via SECM nano and micro-positioning systems, guarantees the achievement of high spatial resolution. SECM is extremely versatile and is widely used for the investigation of numerous processes, such as corrosion [27], electrocatalysis [28], and for the study of biological systems [29–31]. In the field of membrane permeability processes, SECM was previously used by Jadi et al. [32] to explore the morphology and physicochemical features of Nafion/polyaniline composite membranes, meant to be used as solid electrolytes in direct methanol fuel cells. Jadi and colleagues performed SECM measurements using a microelectrode as a probe to check through cyclic voltammetry the permeation of methanol at a fixed distance (100 μm) from the membrane between two points (center and outer zone of the target). Previously, Scott and colleagues [33] determined the porosity of mica membranes and imaged potassium ferrocyanide flux through 1.3 μm pores in the mica membrane. The study confirmed that the pretreatment of the Nafion membrane with polyaniline reduced the methanol crossover. In the field of redox flow batteries, SECM was principally used *i)* to quantify the rates of molecular transport through porous films on conductive substrates in polymer-based RFBs, [34] as these batteries lifetime is correlated to the uptake of ions into the polymeric film, or *ii)* it was coupled with in situ Raman spectroscopy to quantify the chemical rates of decomposition and to identify the reaction intermediates of redox active molecules that constitute the anolyte/catholyte in non-aqueous RFBs [35]. To the best of our knowledge, SECM has not been applied so far to study permeation of membranes employed as separators in RFBs. The aim of the present contribution is to develop a novel procedure to investigate the permeability of separators for RFBs. The method described here allows us to measure concentration profiles of the active species permeating through the membrane as a function of both distance from the membrane and time, enabling us to disentangle the various processes occurring across space and time. This knowledge is crucial for understanding the effects of species permeation and must be considered when designing electrochemical cells - for example, in deciding the optimal electrode-separator distance or shaping electrode geometry. To the best of our knowledge, this is the first example of using concentration profiles obtained through SECM scans to evaluate the permeability performance of a membrane designed for redox flow battery applications.

To showcase its viability, SECM was used as the principal tool to investigate and characterize the crossover of cupric ions through commercial and modified membranes meant to be used in the construction of a copper-based redox flow battery (CuRFB), here considered as a case study. In this technology, when charging the battery, the electrochemical conversion of cuprous cation to cupric cation occurs in the positive compartment as showed in the reaction (1), while in the negative compartment the metallic copper deposition takes place, as for reaction (2). The reverse reactions occur upon discharge.

$$+)\mathrm{Cu}^{2+} + \mathrm{e}^- \underset{\text{charge}}{\overset{\text{discharge}}{\rightleftharpoons}} \mathrm{Cu}^+ \quad (1)$$

$$-)Cu^0 \overset{\text{discharge}}{\underset{\text{charge}}{\rightleftharpoons}} Cu^+ + e^- \quad (2)$$

During battery charge, the Cu^{2+} permeation in the negative half-cell leads to the dissolution of the copper deposit according to the comproportionating reaction (3), which results in the battery's self-discharge and in the unbalance of the electrolyte [36,37].

$$Cu^{2+} + Cu^0 \rightleftharpoons 2Cu^+ \quad (3)$$

In previous studies on CuRFB system, a low-cost porous separator like Daramic was used, but the low selectivity led to high self-discharge rates (e.g., 3 mA cm^{-2} at 50 % SOC) and charge imbalance, requiring operation at >50 mA cm^{-2} for acceptable current efficiency (CE) at the cost of reduced energy efficiency (EE) [22]. To address these issues, IEMs were evaluated as alternatives in CuRFB. The FAP-330 AEM demonstrated higher conductivity (12 mS cm^{-1} in 0.5 M H_2SO_4, lower thickness (27–33 μm), and significantly improved CE (>85 %) by reducing Cu^{2+} crossover. As a result, the FAP-330 membrane achieved an average EE of 73 %, higher than Daramic (47 %) [38]. SPEEK-modified membranes have been investigated to evaluate the feasibility of an in-house method for improving porous membranes. SPEEK was chosen as a promising alternative to traditional perfluorosulfonic acid membranes due to its exceptional thermal stability, robust mechanical properties, and adjustable proton conductivity [21,39,40].

We designed a specific electrochemical cell in which the membrane separates copper(II) chloride and calcium chloride solutions. We performed cyclic voltammetries (CVs) with a Pt microelectrode at a fixed distance from the membrane in a calcium chloride solution. Additionally, probe scan curves (PSCs) were used to spatially resolve the concentration of the permeating cupric ion in the calcium chloride solution, resulting from their diffusion through the separator. We interpreted the behavior of the different membrane types in terms of ion permeability and hydrophobic features by matching the experimental results with quantitative simulation of the diffusional properties of the separators with finite elements simulations.

2. Experimental section/methods

Materials. Copper (II) chloride dehydrates (99.99 + %) and calcium chloride (≥99 %, ACS reagent) were purchased from Merck. The reagents were used to prepare 0.05 M solutions in deionized water. The list of commercial and modified membranes studied in the present work is reported in Table 1, where also the measured wet and dry membrane thicknesses are reported. Membrane modifications with sulfonated polyether ether ketone (SPEEK) have been previously described in the literature [40]. Daramic® supports were cut and coated with solutions containing sulfonated polyether-SPEEK to obtain loadings of 50 and 100 %. To prepare the SPEEK membranes, 12.5 % wt % solid SPEEK was added into 10 mL DMF vials and magnetically stirred for 24 h to form homogeneous solutions suitable for casting. The solution was cast on the Daramic membrane and left drying for 24 h in air and then put in the oven at 80 °C for 24 h. These membranes are named Dar-SP50 and Dar-SP100.

Electrochemical Instrumentation. All electrochemical measurements were carried out with an electrochemical workstation 910B SECM (CH Instruments) coupled with a Nikon ECLIPSE *Ti* (phase contrast and fluorescence) inverted optical microscope. The stepper motors and the piezoelectric components of the 910B CHI instrument for the microelectrode positioning were removed from the original stage and mounted on the plate of the inverted microscope.

Electrochemical cell and electrodes. A SECM cell was specifically designed to separate the two different solutions of the half-cells with a membrane, as reported in Fig. 1A. The solutions were not in contact, and any passage of the ions from one compartment to the other could only occur through the membrane. The bottom part of the cell was filled with 0.05 M $CuCl_2$ solution as a copper source, while the upper part of the cell was filled with 0.05 mM $CaCl_2$. Equal concentration contributes to minimizing the osmotic contribution to mass transport.

Electrochemical measurements were carried out in three-electrode configuration, comprising a 10 μm diameter Pt disk microelectrode (CHI116 10 μm diameter Pt SECM tip) as working electrode (WE), a platinum wire as counter electrode (CE) and an Ag/AgCl (KCl 3 M)

Table 1
List of the tested membranes.

Label	Membrane	Type	$Thickness_{dry}$	$Thickness_{wet}$	Supplier
Dar	Daramic	Porous	900 μm	900 μm	Daramic®
FAP330	Fuma Tech FAP-330	AEM	33 μm	40 μm	Fuma Tech
FS950	Fuma Tech FS-950	CEM	50 μm	60 μm	Fuma Tech
Dar-SP50	Daramic+SPEEK	Porous+CEM	1143 μm	1147 μm	
Dar-SP100	Daramic+SPEEK	Porous+CEM	1026	1010	-

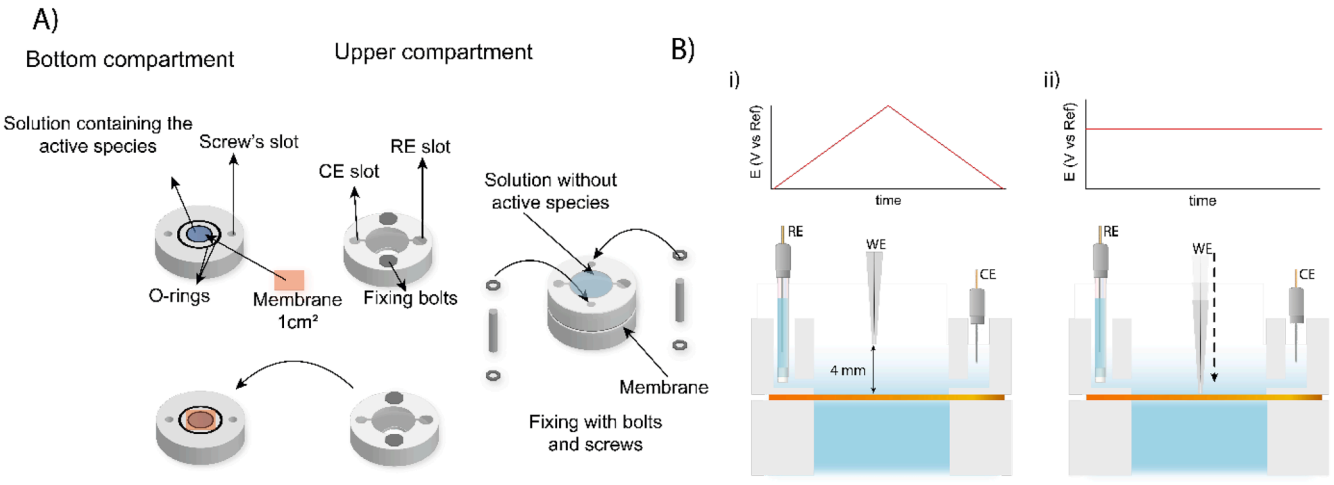

Fig. 1. (A) Scheme of SECM electrochemical cell and (B) SECM configuration used to study the membranes.

(CHI111 Ag/AgCl Reference Electrode w/ porous Teflon Tip) as reference electrode. The microelectrode was polished prior to use with abrasive diamond paper on a glass support, followed by sonication for some seconds in a sonicator bath. Counter electrode was polished with alumina (diameter 1 μm and 0.05 μm) and deionized water before use. The measurements were repeated at successive times for each of the six investigated membranes.

Electrochemical measurements. The permeation of the species is followed as a function of the faradic current due to the permeated species recorded at the microelectrode. Cyclic voltammetries (CVs) were performed with the probe in the upper solution (0.05 M $CaCl_2$) at 4 mm distance (z axis direction, perpendicular respect to the electrochemical cell) from the membrane, to investigate the Cu^{2+} permeation through the membrane into the bulk of the solution (Fig. 1B-i). The potential range used for CVs was −0.4 to 0.8 V vs Ag/AgCl (3 M KCl). PSCs were recorded at 25 μm s^{-1} with the microelectrode in the upper solution (0.05 M $CaCl_2$) at the potential of 0.1 V vs Ag/AgCl (3 M KCl) starting from 4 mm of distance and approaching the surface of the membrane (Fig. 1B-ii). The approach curves were measured at the center of the membrane. All the data were elaborated using Origin 9 Pro program and cut at the distance of 2 mm. The spatial resolution is 0.5 μm and the time resolution is 20 ms.

Contact Angle Measurements. Static contact angle measurements were performed on the selected membranes using a KSV CAM101 instrument under ambient conditions by recording the side profiles of electrolyte drops for image analysis. The shape of the drop was recorded in a time range of 10 s by collecting an image every 0.2 ms. At least five drops for each sample were tested.

Finite Element Simulations. Finite element simulations of copper diffusion across Dar and Dar-SP100 membranes were performed with COMSOL Multiphysics software 6.0. A planar section of the electrochemical cell was modelled considering Dar and Dar-SP100 membranes thickness. The Model Builder tool of COMSOL was employed to define geometries of the model as shown in **Fig. S1A**: the lower and upper compartments of the electrochemical cells had lateral dimension and height of 10 mm, while the thickness of the separators was defined in accordance with the thickness of Dar and Dar-SP100 membranes measured in wet conditions (Table 1). Initial conditions were set in accordance with the experimental measurement, with [Cu(II)] = 50 mM in the lower compartment and [Cu(II)] = 0 in the upper compartment of the electrochemical cell. Diffusion of copper was simulated using the time dependent modelling for the "Transport of diluted species" physics as defined in the COMSOL software. In particular, the general differential formulation of the Fick's Second Law was employed:

$$\frac{\delta c_i}{\delta t} + \nabla \cdot j_i + u \cdot \nabla c_i = R_i \quad (4)$$

$$j_i = -D_i \nabla c_i$$

with the following definitions: c_i the copper concentration at a given point in the space, j_i the flux of copper, u the velocity vector of the fluid, $\nabla \cdot j_i$ the divergence of the flux, D_i the coefficient of diffusion of copper, R_i the reaction rate. No convection was considered in our simulation, thus setting $u = 0$.

Fick equations were solved from 0 to 24 h at defined time points and the copper concentration profiles in the upper compartment were evaluated at the spatial coordinates defined by the red line shown in **Fig. S1C**. Boundary conditions were set with no flux at all the segments of the external perimeter of the geometrical model of the cell (as shown in **Fig. S1D**), while instead flow was allowed at all the remaining boundaries between the various cell compartments and the separators. When solving Fick's second law differential equations, the Backward Differentiation Formula (BDF) solver was employed, with maximal and minimum BDF order of 2 and 1, respectively; Backward Euler initiator was employed with Euler fractional step of 0.001. Tolerances were globally scaled automatically with a 0.1 factor. The diffusion of copper was simulated using the time dependent modelling for the transport of diluted species as defined in COMSOL package. Diffusion coefficient for copper in water $D_m = 1.2 \cdot 10^{-9}$ $m^2 s^{-1}$ in the lower and upper compartments were obtained from the literature [40]; Diffusion coefficient of copper in the membrane compartment instead was adjusted in the simulations to approximate concentration profiles of copper in the upper compartment experimentally obtained at 8 and 24 h. Triangular meshing was defined, with increasing mesh density at the boundaries between the upper compartment and the membrane. Meshing used both for Dar and Dar-SP100 membranes are shown in **Fig. S1B**. Physics-controlled mesh option was enabled for meshing definition, which resulted in homogenous meshing with mesh elements dimensions in the 0.03–0.67 mm for the upper and lower compartments. Mesh densities were increased in the space defined by the separator and the first 2 mm of the upper compartment at the boundary with the separator, to gain better description of the much faster changing copper gradients experimentally seen in these regions. In this latter part, equilateral meshing geometry was applied with the following parameters: minimum-maximal element dimension, 0.0015–0.13 mm; maximal element increase ratio, 1.08; curvature factor, 0.25.

3. Results and discussion

3.1. SECM study of commercial and modified separators

Scanning electrochemical microscopy was used to investigate the permeation of Cu^{2+} species through a variety of commercial and in-house modified membranes, in view of their use as separators in CuRFBs.

Fig. 2A shows CVs recorded 24 h after cell assembly. The presence of redox peaks associated with copper species in the CVs of the bulk solution confirms that Cu^{2+} permeated through the separator from the lower to the upper compartment. The reduction peaks observed between 0.2 V and −0.1 V and from −0.1 V to −0.4 V vs. Ag/AgCl (3 M KCl) are ascribed to the Cu^{2+}/Cu^{+} and Cu^{+}/Cu reduction processes, respectively. The presence of a broad Cu^{2+}/Cu^{+} voltammetric signal suggests that Cu^{+} species are slightly stabilized in solution. It has already been reported that Cu^{+} stabilization is strongly influenced by chloride availability [42]. In the lower compartment of the presented system, where Cu^{2+} is present, its concentration is 50 mM, while chloride concentration is 100 mM, resulting in a Cu:Cl ratio of 1:2. In the upper compartment, the chloride concentration is 100 mM is present, whereas the copper concentration is determined only by the copper species diffusing through the membrane, leading to a significantly higher Cu:Cl ratio (~1:30), which favors Cu^{+} stabilization. The oxidation peak at 0.01 V is attributed to the anodic stripping of copper from the Pt microelectrode surface that produces Cu^{+} as cations absorbed at the electrode ($Cu^{+}_{(ads)}$) and dissolved in solution ($Cu^{+}_{(sol)}$), while redox signals in the 0.1–0.3 V range can be due to the Cu^{+}/Cu^{2+} oxidation processes. The latter consists of two signals that we ascribed to the oxidation of $Cu^{+}_{(ads)}$ and $Cu^{+}_{(sol)}$ to Cu^{2+} [43]. These latter peaks are absent in the CVs of Dar-SP100 and FAP330 membranes (Fig. 2A), likely due to the lower Cu^{2+} concentration reaching the bulk solution in the upper compartment. For the PSC measurements, the potential of 0.1 V vs. Ag/AgCl (3 M KCl) was chosen, as copper deposition does not occur at this potential. This is confirmed by the absence of any current decrease that would have been present if Cu deposition had occurred on the ultramicroelectrode (UME) surface, increasing its effective area. As shown in Fig. 2B, after 24 h a stationary concentration of copper in the upper compartment was measured for all the membrane types. This could be inferred by the shape of PSCs of Fig. 2B, in which the reduction currents did not show a relevant increase at this time point in proximity of the membrane surface (last 100 μm from the membrane surface of PSC) as observed for shorter time points (see for example for the Daramic membrane Figs. 3A and 3B). Reduction currents recorded in the bulk were relevantly different among the membranes. To better appreciate these differences, the corresponding concentration curves are plotted in Fig. S2, by using copper diffusion

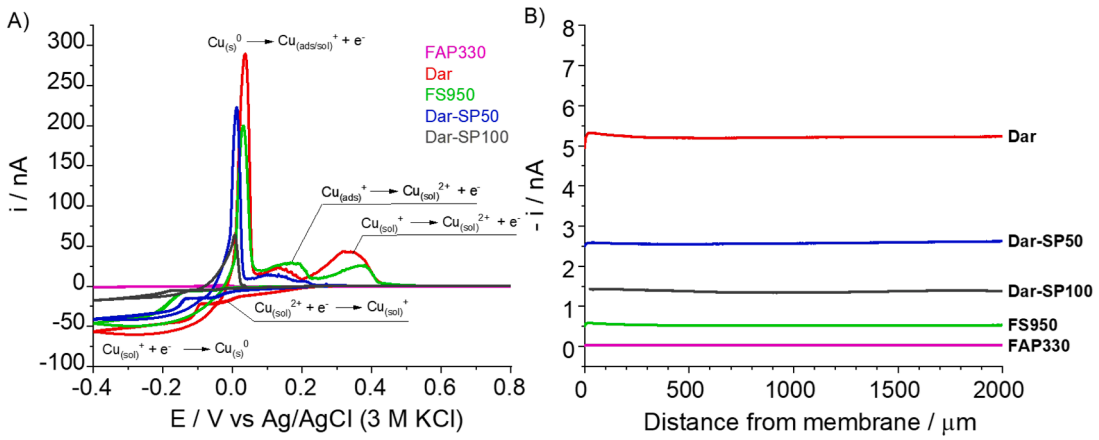

Fig. 2. CVs and PSCs of Pt microelectrode in the SECM cell recorded 24 h after the calcium chloride and copper solutions were placed in contact with the different separators. (A) CVs at 50 mV s^{-1} and 4 mm far from the membrane. (B) PSCs at 25 μm s^{-1}.

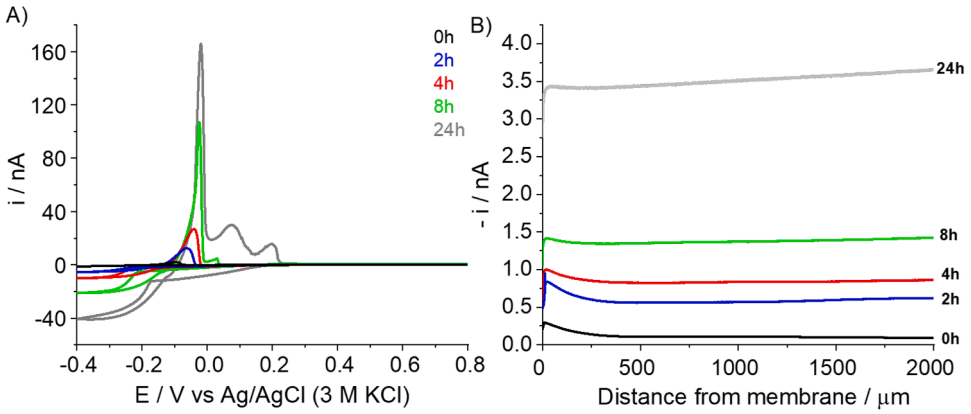

Fig. 3. CVs and PSCs of Pt microelectrode in the SECM cell recorded in time intervals between 0 and 24 h after the calcium chloride and copper solutions were placed in contact with the separator. (A) CVs at 50 mV s^{-1} and 4 mm far from Daramic membrane. (B) PSCs at 25 μm s^{-1}.

coefficient $D_m = 1.2 \cdot 10^{-9}$ $m^2 s^{-1}$ from literature [41] and the steady state equation (eq. S1) of the currents measured with a disk microelectrode. The copper concentration after 24 h was verified by measuring the absorbance at 870 nm of the solutions at the end of the measurements (Table S1). The concentration values are comparable with those evaluated by PSCs. Daramic porous membrane showed the worst performance as separator, as the Cu^{2+} concentration inside the bulk solution after 24 h resulted to be the highest. The lowest copper(II) concentrations were observed for the FAP330, FS950 and Dar-SP100 membranes, as confirmed by CVs in Fig. 2A. Interestingly, Dar-SP100 permeability to Cu^{2+} cations decreased because of modification with SPEEK. The thickness of the SPEEK layer does not seem to play a significant role, as the values measured for wet membranes (Table 1) were not correlated with Cu^{2+} concentrations resulting from SECM in the upper compartment. On the contrary, results could be rationalized in view of some membrane molecular descriptors such as wettability and ion exchange typology. The wettability of the membranes involved in the study was evaluated by contact angle measurements (**Fig. S3-S4**) and considered a relevant parameter in copper cations permeation, as membranes should be wettable to sustain ion conductivity. FAP330 AEM allows anionic transport and hinders cations in crossing the membrane. Additionally, it showed one of the highest contact angles, i.e., around 80–86° (**Fig. S3C**), suggesting high hydrophobicity of its surface, making FAP330 one of the most efficient separators among the tested ones. Dar-SP100 and FS950 allows the passage of cations, as it is appreciable from the CVs and PSCs reported in Fig. 2**A-B**. However, FS950, among the tested membranes, is one of the less wettable, with a contact angle higher than 80° (**Fig. S3B**), which indicates high hydrophobicity of its surface. SPEEK modification also seemed to increase the hydrophobic feature of the Daramic membrane: bare Daramic in fact presented hydrophilic features, with contact angles around 50°, but after SPEEK modification its hydrophobicity increased relevantly (**Fig.s S3A** and **S3D-E**) as suggested by contact angle measurements, which reached 70–75°. These results demonstrate that the best performances as separators measured by SECM for FAP330, FS950 and Dar-SP100 membranes were correlated to lower wettability of these materials, together with ion exchange capability. These results for commercial membranes are consistent with electrochemical test previously performed in the CuRFB system [11,38].

To better investigate the interesting behavior observed for Daramic membranes after SPEEK modification we performed further analyses on Daramic and Dar-SP100 separators.

3.2. *Impact of SPEEK modification on Daramic permeability to cupric cation*

Bare Daramic and its SPEEK-modified counterpart Dar-SP100 were selected to evaluate the potential of SECM for monitoring the diffusion of active species over time. PSCs and CVs were measured at 0, 2, 4, 8 and 24 h from the final assembly of the electrochemical cell. The results for Dar membrane are reported in Fig. 3A, where the CVs showed that Cu^{2+} concentration in the upper compartment of the electrochemical cell gradually increases with time. Currents related to cupric and cuprous reduction processes at negative potentials, below −0.25 V vs Ag/AgCl (3 M KCl), progressively increased from 0 to 24 h, as also those related to

copper stripping process at the electrode, that could be appreciated between 0.01 and −0.04 V vs Ag/AgCl (3 M KCl). The CV recorded at 24 h (Fig. 3A) as compared to that recorded immediately after the assembly of the electrochemical cell (Fig. 3A) shows that Cu^{2+}diffused extensively to the upper compartment, as can be inferred from the Cu^{+}/Cu^{2+}oxidation processes observed at around 0.05–0.25 V vs Ag/AgCl (3 M KCl). All the peaks of CVs are deeply described in Fig. 2A. The additional oxidation peaks visible in 24 h are absent in the CVs recorded at shorter times, likely due to the lower Cu^{2+} concentration reaching the bulk solution in the upper compartment. The PSC (Fig. 3B) recorded by progressively approaching the surface of the Daramic membrane starting from 2 mm from the surface of the separator, reported on the concentration profiles of copper cations established in the upper compartments due to their diffusion in this compartment through the Daramic separator. After 2 h, an increase of current by approaching the separator surface could be clearly measured (the increase started approximately at 300 μm from the substrate) due to the increase of copper ion concentration when getting closer to the copper ion source. The rapid decrease of the currents in close proximity of the membrane is not due to changes in the copper ion concentrations, but is a typical behavior observed in SECM measurements when approaching a physical surface that hinders the redox specie diffusion to the microelectrode probe [44]. In fact, the diffusion of the copper ions in the membrane is much lower than the one in the aqueous media of the measured compartment. This behavior for PSCs, has been largely reported in the literature for other systems [39]. The increase of copper ions near the separator at 2 h supports the hypothesis that initially the Daramic membrane behaved as a reservoir of copper from which copper diffusion takes place. This phenomenon diminishes over time, as the concentration profiles are shaped as expected from the theory of the dilute species diffusion from a donor compartment and through a low diffusion separator membrane. This is evidenced by the PSC at 24 h (Fig. 3B), indicating that stable flux is approximately achieved in the upper compartment by this time. The increase in current over time at 2000 μm is attributed to the concentration increase in the solution. Daramic membrane allows a slow, but not negligible crossing of the cupric ion species.

Finite elements simulations were performed to simulate the overall permeation process and to estimate diffusion coefficients of cupric ion through the Daramic separator. The geometry of the electrochemical cell was simulated as shown in **Fig. S1**. Fig. 4A displays the magnification of the simulated gradients of Cu^{2+}in the system obtained by employing the diffusion constant (*D*) of copper ion in the Daramic separator that best approximated the PSC at 24 h. More details on the characteristics of the simulated systems and on COMSOL modelling analysis are reported in Supplementary Information and in Fig. S5. PSC curves measured from

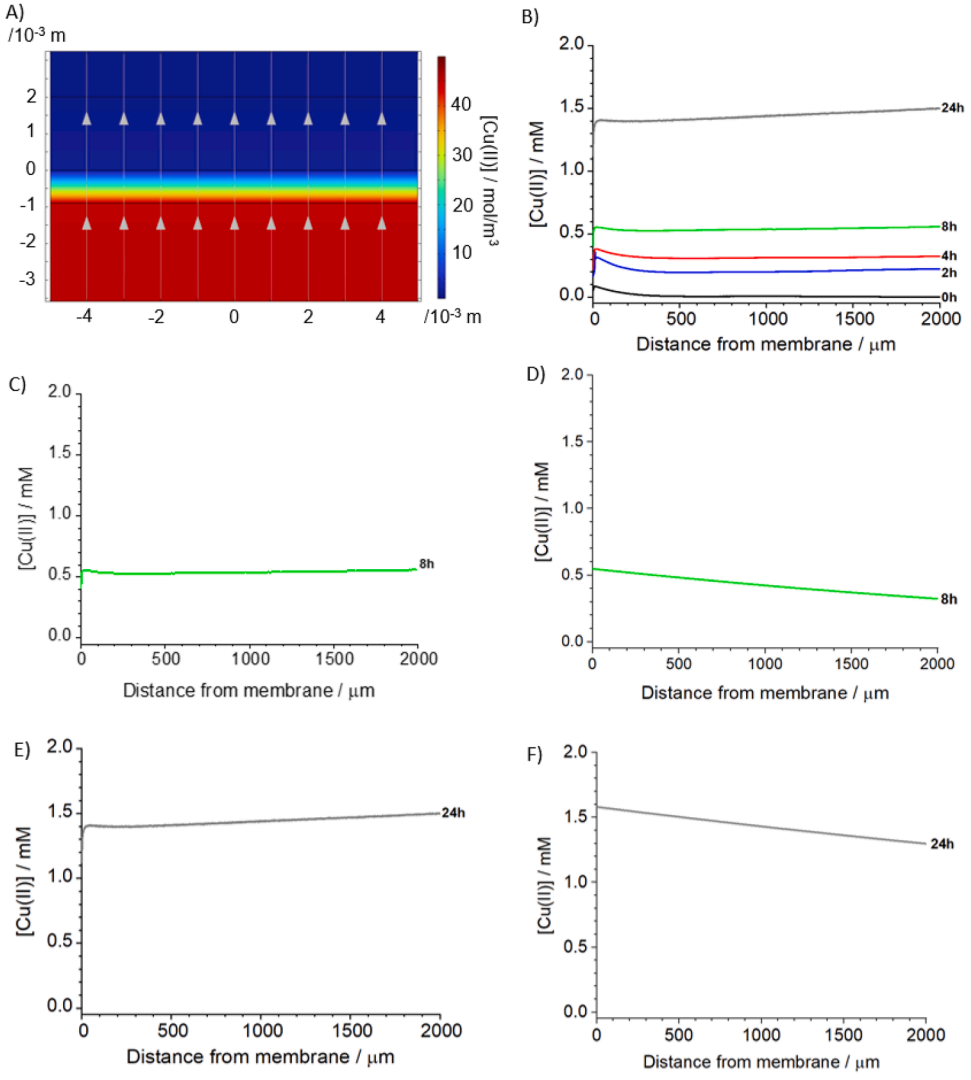

Fig. 4. Simulation of concentration gradients of Cu^{2+} in the proximity of the Daramic separators after 24 h (A). Concentration profiles obtained from PSCs (B). Concentration profiles of Cu^{2+} after 8 h (C) and 24 h (E) and corresponding COMSOL simulations (D,F).

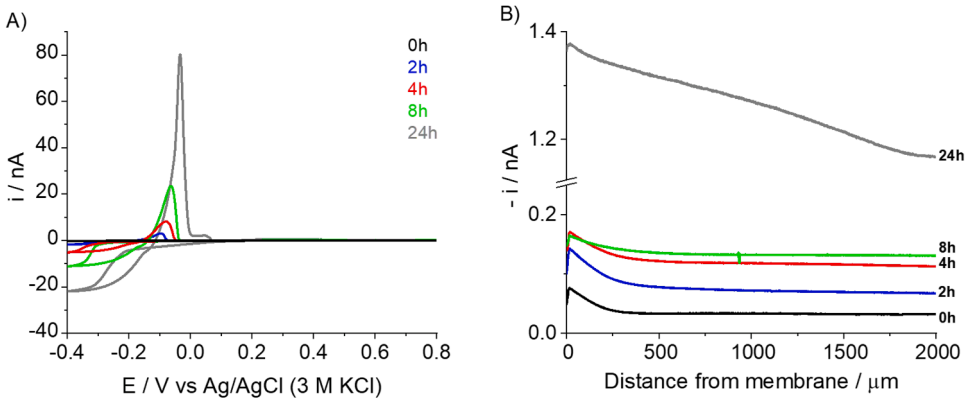

Fig. 5. CVs and PSCs of 10 μm Pt microelectrode in the SECM cell recorded in time intervals between 0 and 24 h after the calcium chloride and copper solutions were placed in contact with the separator. (A) CVs at 50 mV s^{-1} and 4 mm far from Dar-SP100. (B) PSCs at 25 μm s^{-1}.

0 to 24 h are reported in Fig. 4B that shows the number of species that crossed the Daramic membrane progressively increasing over time. Simulations were carried out for finding the diffusion coefficients and, hence, the permeability of copper ions in the Daramic separators. The simulations were iteratively refined to accurately reproduce the concentration profiles measured by SECM. The lower and upper value of the diffusion coefficient ranges were determined as the *D* values that best approximate PSC at 8 and 24 h (Fig. 4C and 4E) in the first 200 μm far from the separator in the upper compartment of the cell. Residual difference between the PSC and the modelled copper concentration profiles were minimized, and we obtained from a minimum of 0.001 mM to 0.05 mM residual discrepancies for the four *D* estimated (Dar and Dar-SP100 at 8 and 24 h). The value of $D = 4{\cdot}10^{-12}$ m^2s^{-1} was estimated as the one that best approximated PSC at 8 h (Fig. 4D), while $D = 5{\cdot}10^{-12}$ m^2s^{-1} (Fig. 4F) best approximated PSC experimentally measured at 24 h.

Fig. 5 shows the results of SECM analysis of Dar-SP100. The CVs

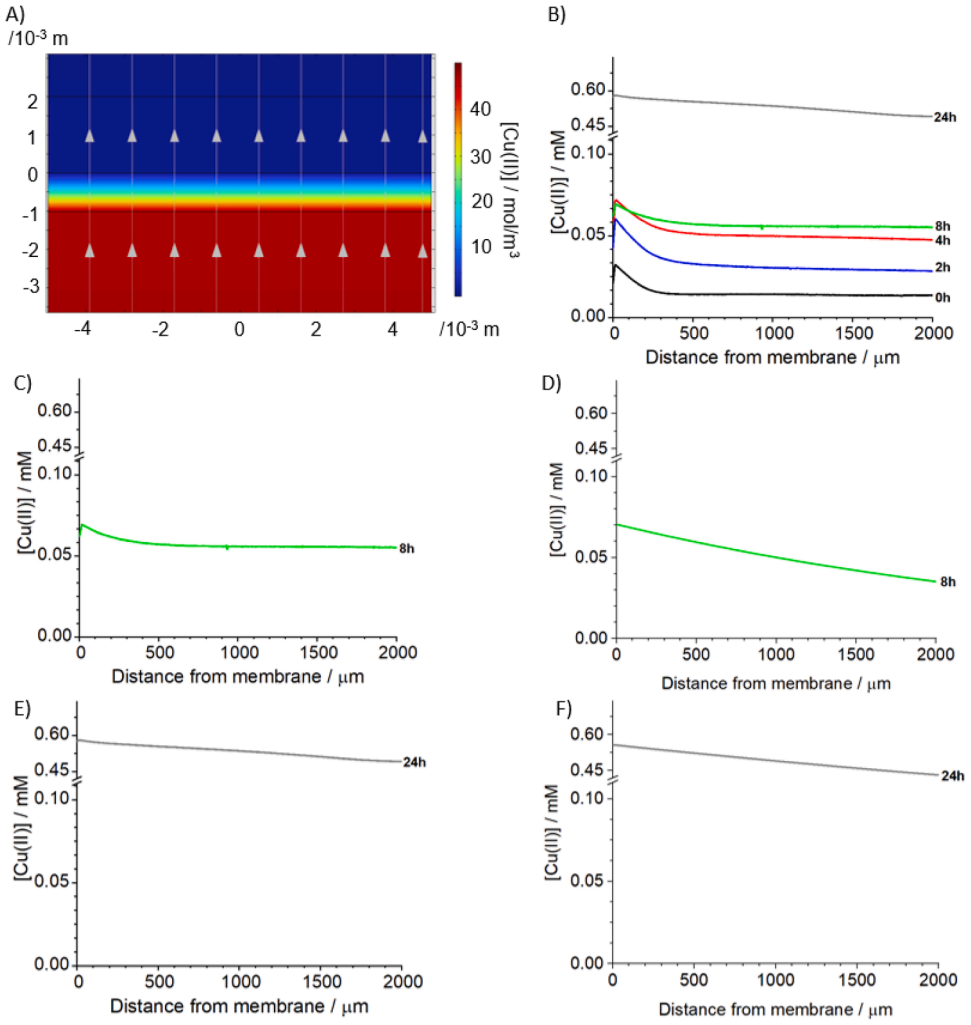

Fig. 6. Simulation of concentration gradients of Cu^{2+} in the proximity of the Dar-SP100 separators after 24 h (A). Concentration profiles obtained from PSCs (B). Concentration profiles of Cu^{2+} after 8 h (C) and 24 h (E) and corresponding COMSOL simulations (D,F).

Table 2
Ranges of copper ion diffusion coefficients, permeabilities and accumulation rates at 24 h and 2 mm far from the membrane in the upper compartment for Dar and Dar-SP100.

Membrane	Diffusion coefficient, D / $10^{-12}m^2s^{-1}$	Permeability, P / $10^{-9}ms^{-1}$	$\frac{d[Cu(II)]}{dt}(2mm, 24h)$, / μMh^{-1}
Dar	4 ÷ 5	4 ÷ 6	70÷ 90
Dar-SP100	2.5 ÷ 3	2.5 ÷ 3	30÷40

recorded in the bulk solution from 0 to 24 h from the complete assembly of the electrochemical cell are reported in Fig. 5A. Both reduction and oxidation currents in general were lower than those recorded in the presence of the bare Daramic membrane. The CV after 24 h, in addition to the typical deposition-stripping signals, shows only the oxidation peak attributed to the oxidation of the $Cu^{+}_{(ads)}$ to Cu^{2+}, as already seen in Fig. 2A. This behavior can be attributed to lower amounts of Cu^{2+}that pass through the Dar-SP100 from the $CuCl_2$ solution in the lower compartment towards the upper one. As mentioned before, the SPEEK modification limits the Daramic membrane wettability, thus influencing the charge carrying. For all the tested membranes, the reduction current of Cu^{2+}reaches the highest value after 24 h (Fig. 5A). This result was also confirmed by the PSC recorded at 0.1 V vs Ag/AgCl (3 M KCl) at the same time point of the CVs (Fig. 5B). It is worth noting that for the first 8 h the approach curves show a slight increase of the reduction currents while the Pt working microelectrodes get closer to the membrane surface. The increase of the bulk currents measured far from the membrane was smaller than those measured for the bare Daramic membrane, as evident also from CVs. This emphasizes the lower permeability of this membrane to the active species. The curve recorded after 24 h (Fig. 5B) shows that the bulk reduction currents relevantly increased as compared to previous time points; this can be attributed to the increased hydrophobicity of the Daramic membrane after the SPEEK modification.

Fig. 6A reports the copper concentration gradients simulated for Dar-SP100 separator at 24 h. As shown in Fig. 6B, the concentration of the copper species in the upper compartment is relatively low and the currents increase gradually as the substrate is approached. PSCs and the correspondent COMSOL simulations at 8 and 24 h are reported in Figs. 6C-E and 6D-F, respectively. The concentration profile at 24 h did not change from the bulk to the surface of the membrane, indicating that the system approximately reached equilibrium. COMSOL simulations returned a range of D values that best approximate 8- and 24-hours PSCs of $2.5{\cdot}10^{-12}$ and $3{\cdot}10^{-12}$ m^2s^{-1}.

In summary, the presented method gave a direct measurement of the copper concentration profiles for the Dar and Dar-SP100 separators and a quantitative comparison of copper diffusion coefficients and permeabilities in the two membranes, as summarized in Table 2, where the ranges of these values are reported. In addition, we evaluated the accumulation rate of the copper ions at 2 mm from the membrane at 24 h $\left(\frac{d[Cu^{2+}]}{dt}(2mm, 24h)\right)$, as reported in the Table 2.

The simulation results are consistent with the experimental observations, and as expected the SPEEK coating on the Daramic results in a beneficial impact reducing the membrane permeability to Cu^{2+}. Moreover, they offer a powerful tool to explore the system behavior in timeframes that are experimentally inaccessible, thus extending the insight beyond the limits of direct measurements.

4. Conclusions

All RFBs are affected by self-discharge issues when active species cross the membrane of the cell. For this reason, the performance as separators of membranes used in redox flow batteries are important to prevent this phenomenon. In our investigation, we developed a new method to investigate membrane permeability to specific active species. The presented method integrates a dual-compartment electrochemical cell tailored for the selective detection of Cu^{2+} ions migrating across different membranes. This setup, along with time-resolved probe scans and voltammetric measurements, enabled a direct and spatially resolved assessment of active species crossover.

Among the tested membranes, FAP330, FS950, and Dar-SP100 showed the most effective suppression of Cu^{2+} transport over 24 h, correlating with their surface hydrophilicity as evaluated via contact angle measurements. Furthermore, the SPEEK-modified Daramic membrane exhibited improved retention capabilities, highlighting the benefit of targeted surface modification.

To complement the experimental findings, finite element method (FEM) simulations were used to estimate the diffusion coefficients of Cu^{2+} through selected membranes. These simulations, based on experimental probe current profiles and temporal evolution of concentration gradients, allowed a quantitative comparison between bare and modified membranes. Specifically, the diffusion coefficient derived for the SPEEK-modified Daramic membrane was significantly lower than that of the unmodified counterpart, confirming the impact of the modification. While additional validation and refinement of the simulation model are ongoing, these preliminary results support the potential of FEM as a complementary tool for separator evaluation.

This work proves that the integration of SECM analyses and finite element simulations is a powerful approach to support the choice and the development of separators, which could enable relevant improvements in the efficiency of the redox flow batteries.

CRediT authorship contribution statement

Simona De Zio: Writing – original draft, Investigation, Data curation. **Giampaolo Lacarbonara:** Writing – original draft, Investigation, Data curation. **Wouter Badenhorst:** Investigation, Resources, Software. **Marco Malferrari:** Writing – review & editing, Investigation, Formal analysis, Data curation. **Rossella Petruzzelli:** Investigation. **Lasse Murtomäki:** Writing – review & editing, Supervision, Funding acquisition. **Catia Arbizzani:** Writing – review & editing, Supervision, Funding acquisition. **Stefania Rapino:** Writing – review & editing, Supervision, Funding acquisition, Conceptualization.

Declaration of competing interest

The authors declare that they have no known competing financial interests or personal relationships that could have appeared to influence the work reported in this paper.

Acknowledgements

This work was supported by the European project CUBER Copper-Based Flow Battery for Energy storage Renewables integration (H2020 –LC-BAT_2019 [2020–2024]) under grant agreement No 875605. The Authors thank the Polymer Science and Biomaterials Laboratory for the use of the contact angle measurement apparatus. Simona De Zio, Giampaolo Lacarbonara and Wouter Badenhorst contributed equally to this work.

Supplementary materials

Supplementary material associated with this article can be found, in the online version, at doi:10.1016/j.electacta.2025.146468.

Data availability

Data will be made available on request.

References

[1] J. Noack, M. Skyllas-Kazacos, L. Thaller, G. Tomazic, B. Jonshagen, P. Morrissey, Flow Batteries: From Fundamentals to Applications, vol.2, Wiley-VCH GmbH, Weinheim, 2023, pp. 29–52, https://doi.org/10.1002/9783527832767.ch2.

[2] L. Sanz, D. Lloyd, E. Magdalena, J. Palma, K. Kontturi, J. Power. Sources. 268 (2014) 121, https://doi.org/10.1016/j.jpowsour.2014.06.008.

[3] S. Roe, C. Menictas, M. Skyllas-Kazacos, J. Electrochem. Soc. 163 (2016) A5023, https://doi.org/10.1149/2.0041601jes.

[4] L. Zhang, Q. Lai, J. Zhang, H. Zhang, ChemSusChem. 5 (2012) 867, https://doi.org/10.1002/cssc.201100530.

[5] H.S. Lim, A.M. Lackner, R.C. Knechtli, J. Electrochem. Soc. 124 (1977) 1154, https://doi.org/10.1149/1.2133517.

[6] A. Khor, P. Leung, M.R. Mohamed, C. Flox, Q. Xu, L. An, R.G.A. Wills, J.R. Morante, A.A. Shah, Mater. Today Energy 8 (2018) 80, https://doi.org/10.1016/j.mtener.2017.12.012.

[7] K. Amini, M.D. Pritzker, Appl. Energy 255 (2019) 113894, https://doi.org/10.1016/j.apenergy.2019.113894.

[8] X. Li, Electrochim. Acta 170 (2015) 98, https://doi.org/10.1016/j.electacta.2015.04.075.

[9] M.C. Tucker, A. Phillips, A.Z. Weber, ChemSusChem. 8 (2015) 3996, https://doi.org/10.1002/cssc.201500845.

[10] B. Schwenzer, J. Zhang, S. Kim, L. Li, J. Liu, Z. Yang, ChemSusChem. 4 (2011,) 1388, https://doi.org/10.1002/cssc.201100068.

[11] T. Mohammadi, M. Skyllas-Kazacos, J. Memb. Sci. 98 (1995) 77, https://doi.org/10.1016/0376-7388(94)00178-2.

[12] T. Xu, J. Memb. Sci. 263 (2005) 1, https://doi.org/10.1016/j.memsci.2005.05.002.

[13] I.A. Stenina, A.B. Yaroslavtsev, Membranes. (Basel) 11 (3) (2021) 198, https://doi.org/10.3390/membranes11030198.

[14] T. Kyu, *ACS Symposium Series*, 1985, pp. 365–405, https://doi.org/10.1021/bk-1985-0269.ch018.

[15] H. Prifti, A. Parasuraman, S. Winardi, T.M. Lim, M. Skyllas-Kazacos, Membranes. (Basel) 2 (2012) 275, https://doi.org/10.3390/membranes2020275.

[16] C. Chen, Y.-L.S. Tse, G.E. Lindberg, C. Knight, G.A. Voth, J. Am. Chem. Soc. 138 (2016) 991–1000, https://doi.org/10.1021/jacs.5b11951.

[17] T. Mohammadi, S.C. Chieng, M. Skyllas Kazacos, J. Memb. Sci 133 (1997) 151, https://doi.org/10.1016/S0376-7388(97)00092-6.

[18] T. Mohammadi, M. Skyllas Kazacos, J. Appl. Electrochem. 27 (1997) 153, https://doi.org/10.1023/A:1018495722379.

[19] T. Sukkar, M. Skyllas-Kazacos, J. Memb. Sci 222 (2003) 235, https://doi.org/10.1016/S0376-7388(03)00309-0.

[20] H. Prifti, A. Parasuraman, S. Winardi, T.M. Lim, M. Skyllas-Kazacos, Membranes. (Basel) 2 (2012) 275–306, https://doi.org/10.3390/membranes2020275.

[21] Z. Mai, H. Zhang, X. Li, C. Bi, H. Dai, J. Power. Sources. 196 (1) (2011) 482–487, https://doi.org/10.1016/j.jpowsour.2010.07.028.

[22] D. Lloyd, E. Magdalena, L. Sanz, L. Murtomäki, K. Kontturi, J. Power. Sources. 292 (2015) 87, https://doi.org/10.1016/j.jpowsour.2015.04.176.

[23] E. Bai, H. Zhu, C. Sun, G. Liu, X. Xie, C. Xu, S. Wu, Membranes. (Basel) 13 (2023) 820, https://doi.org/10.3390/membranes13100820.

[24] M. Gao, M. Salla, F. Zhang, Y. Zhi, Q. Wang, J. Power. Sources. 527 (2022) 231180, https://doi.org/10.1016/j.jpowsour.2022.231180.

[25] H. Vafiadis, M. Skyllas-Kazacos, J. Memb. Sci. 279 (2006) 394, https://doi.org/10.1016/j.memsci.2005.12.028.

[26] P. Sun, F.O. Laforge, M.V. Mirkin, Phys. Chem. Chem. Phys. 9 (2007) 802, https://doi.org/10.1039/B612259K.

[27] D.-H. Xia, J. Wang, Z. Wu, Z. Qin, L. Xu, W. Hu, Y. Behnamian, J.-L. Luo, Sensors Actuators B Chem 280 (2019) 235, https://doi.org/10.1016/j.snb.2018.10.051.

[28] J. Kim, C. Renault, N. Nioradze, N. Arroyo-Currás, K.C. Leonard, A.J. Bard, J. Am. Chem. Soc. 138 (2016) 8560, https://doi.org/10.1021/jacs.6b03980.

[29] S. De Zio, M. Becconi, A. Soldà, M. Malferrari, A. Lesch, S. Rapino, Bioelectrochemistry. 150 (2023), https://doi.org/10.1016/j.bioelechem.2022.108343.

[30] M. Becconi, S. De Zio, F. Falciani, M. Santamaria, M. Malferrari, S. Rapino, Cancers. (Basel) (2023) 15, https://doi.org/10.3390/cancers15041327.

[31] T.E. Lin, S. Rapino, H.H. Girault, A. Lesch, Chem. Sci. 9 (2018) 4546, https://doi.org/10.1039/C8SC01035H.

[32] S. Ben Jadi, A. El Guerraf, A. Kiss, A. El Azrak, E.A. Bazzaoui, R. Wang, J.I. Martins, M. Bazzaoui, J. Solid. State Electrochem. 24 (2020) 1551, https://doi.org/10.1007/s10008-020-04659-2.

[33] E.R. Scott, H.S. White, J.Bradley Phipps, J. Memb. Sci. 58 (1991) 71, https://doi.org/10.1016/S0376-7388(00)80638-9.

[34] M.E. Williams, K.J. Stevenson, A.M. Massari, J.T. Hupp, Anal. Chem. 72 (2000) 3122, https://doi.org/10.1021/ac9914622.

[35] A.S. Danis, M.J. Counihan, K.O. Hatfield, J. Zhang, G. Agarwal, L. Zhang, R. S. Assary, J. Rodríguez-López, Electrochim. Acta 447 (2023) 142123, https://doi.org/10.1016/j.electacta.2023.142123.

[36] G. Lacarbonara, L. Faggiano, S. Porcu, P.C. Ricci, S. Rapino, D.P. Casey, J.F. Rohan, C. Arbizzani, Batteries. (Basel) 7 (2021) 83, https://doi.org/10.3390/batteries7040083.

[37] L. Faggiano, G. Lacarbonara, W.D. Badenhorst, L. Murtomäki, L. Sanz, C. Arbizzani, J. Power. Sources. 520 (2022) 230846, https://doi.org/10.1016/j.jpowsour.2021.230846.

[38] W.D. Badenhorst, L.Sanz Kuldeep, C. Arbizzani, L. Murtomäki, Energy Reports 8 (2022) 8690–8700, https://doi.org/10.1016/j.egyr.2022.06.075.

[39] X. Li, T. Ye, X. Meng, D. He, L. Li, K. Song, J. Jiang, C. Sun, Polymers. (Basel) 16 (19) (2024) 2840, https://doi.org/10.3390/polym16192840.

[40] W. Badenhorst, J.A.Manzanares Kuldeep, L. Murtomäki, Langmuir. 40 (14) (2024) 7512–7519, https://doi.org/10.1021/acs.langmuir.4c00027.

[41] A.C.F. Ribeiro, M.A. Esteso, V.M.M. Lobo, A.J.M. Valente, S.M.N. Simões, A.J.F. N. Sobral, H.D. Burrows, J. Chem. Eng. Data 50 (2005) 1986, https://doi.org/10.1021/JE050220Y.

[42] P. Peljo, D. Lloyd, N. Doan, M. Majanevaa, K. Kontturi, Phys. Chem. Chem. Phys. 16 (2014) 2831–2835, https://doi.org/10.1039/C3CP54585G.

[43] K. Shi, K. Hu, S. Wang, C.-Y. Lau, K.-K. Shiu, Electrochim. Acta 52 (19) (2007) 5907–5913, https://doi.org/10.1016/j.electacta.2007.03.028.

[44] G. Wittstock, M. Burchardt, S.E. Pust, Y. Shen, C. Zhao, Angew. Chemie - Int. Ed. 46 (2007) 1584, https://doi.org/10.1002/anie.200602750.